WELDING RESEARCH

SUPPLEMENT TO THE WELDING JOURNAL, JUNE 1986

Sponsored by the American Welding Society and the Welding Research Council

Readers are advised that all papers published in the *Welding Journal's* Research Supplement undergo Peer Review before publication for: 1) originality of the contribution; 2) technical value to the welding community; 3) prior publication of the material being reviewed; 4) proper credit to others working in the same area; and 5) justification of the conclusions based on the results.

The names of the more than 160 individuals serving on the AWS Peer Review Panel are published periodically. All are experts in their respective technical areas, and all are volunteers in the program.

The Role of Inclusions in Controlling HSLA Steel Weld Microstructures

Nucleation of acicular ferrite is accelerated when there is a combination of large austenite grains and a high density of intragranular inclusions

BY S. LIU AND D. L. OLSON

ABSTRACT. The effects of inclusions on acicular ferrite formation in niobium microalloyed steel submerged arc weld metal were investigated using experimental chemical reagent grade fluxes from the CaF_2-CaO-SiO_2 system. Five different electrode wires were used. Direct relationships between (1) weld metal oxygen and inclusion content and (2) inclusion density and weld metal microstructure were established in this investigation, explaining why it is possible to relate microstructure to weld metal oxygen content, although the inclusion density correlation would be fundamentally more correct. Finer particles and larger size variations were seen in the high oxygen weld metal. The mean particle size of the weld metal inclusions decreased with increasing concentration of oxygen. Inclusions were found located at the grain boundaries or within the austenite grains. Depending on the size distribution, the partition of the inclusions to the boundary and to the interior of the grains may be different. An optimum inclusion size distribution to obtain a large volume fraction of acicular ferrite is the one that contains a low percentage of fine size particles, with the inclusion population sizes resembling a normal, or close to normal, distribution. The combination of large austenite grains and high intragranular inclusion density is the key to obtaining a refined microstructure. The strain energy contribution to the total free energy of austenite decomposition due to the inclusion/matrix differential thermal contraction effect was found to be insignificant when compared with the austenite to ferrite transformation volume free energy term.

Paper presented at the 66th Annual AWS Meeting, held April 29 to May 3, 1985, in Las Vegas, Nev.

S. LIU is with the Department of Industrial Engineering, Pennsylvania State University, University Park, Pa. D. L. OLSON is with the Center for Welding Research, Department of Metallurgical Engineering, Colorado School of Mines, Golden, Colo.

Introduction

Factors affecting HSLA steel weld metal toughness have been studied, and acicular ferrite was found to be the constituent responsible for the high toughness (Refs. 1-6). Acicular ferrite is randomly oriented short ferrite needles which are formed intragranularly. The interlocking nature of acicular ferrite, together with its fine grain size, provides the maximum resistance to crack propagation by cleavage. For this reason, it has become increasingly important to understand the factors which would maximize the volume fraction of acicular ferrite in the weld metal.

In addition to the hardenability agents, such as carbon, manganese, chromium, etc., weld metal oxygen also affects the microstructures and the mechanical properties of steel weld metal. Oxygen can exist in a metal in the form of solid solution element, or in a combined form as inclusions. Due to the low oxygen solubility in iron, only very low free oxygen content, *i.e.*, in the uncombined state, can be expected. A major amount of the oxygen is present as oxide or oxy-sulfide inclusions resulting from reactions of oxygen with iron alloying elements such as silicon, manganese and aluminum in the molten weld pool. In the submerged arc welding process, when

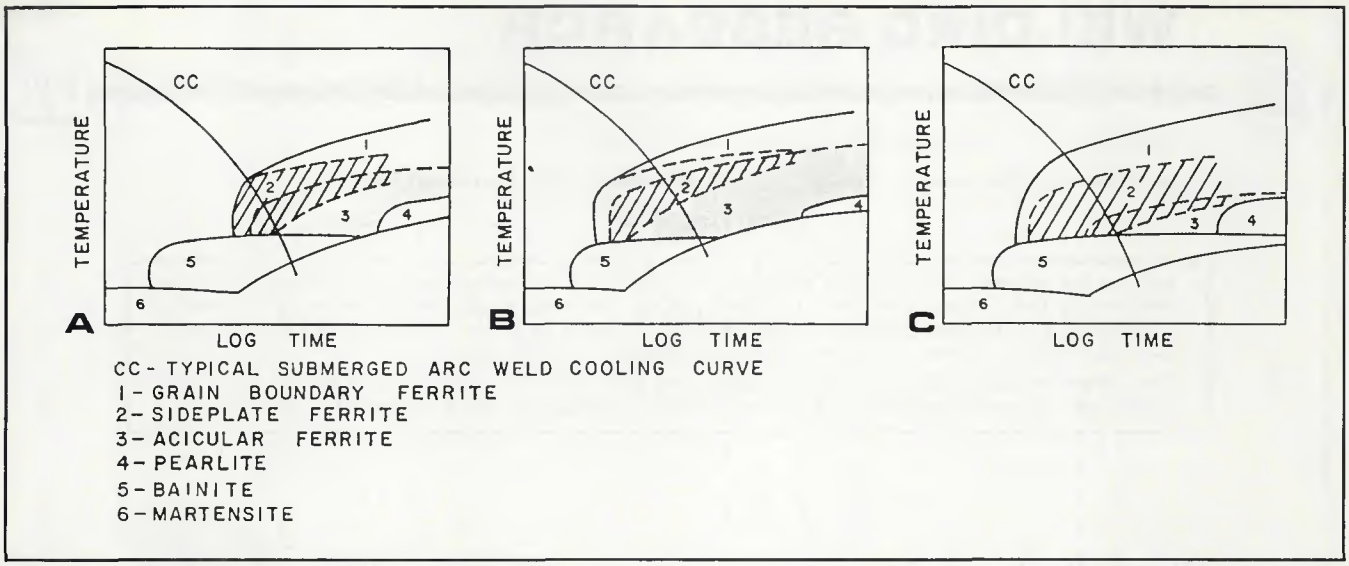

Fig. 1 — Schematic CCT diagrams showing the influence of oxygen on the weld metal phase transformations. A — High oxygen regime; B — Medium oxygen regime; C — Low oxygen regime

given enough time, the inclusions will grow in the melt and separate from the bulk of the weld pool to the layer of molten slag covering the weld puddle. The separation of slags can take place as a result of weld pool fluid flow or particle flotation (Refs. 7, 8). However, solidification in submerged arc weld metal is extremely fast and inclusions may become trapped. The presence of these second phase particles will affect both the mechanical properties and the phase transformation of the weld metal.

In the early 1960's, investigators (Refs. 9–13) determined that mild steel weld metal contained nonmetallic inclusions of sizes ranging from a few tenths to several microns. Most of the inclusions were observed to be oxides and spherical in shape. An alignment of inclusions in rows suggested that they were formed prior to or during solidification (depending on the alloy composition). In the early 1970's, Boniszewski (Ref. 14) did electron diffraction studies of carbon extraction replicas from mild steel weld metal and determined that fine particles (0.005–0.060 micron) were cubic spinel $MnO \cdot Fe_2O_3$ mixed with some Fe_2SiO_4 cubic silicate.

However, it was not until the late 1970's that the problem of weld metal inclusions affecting ferrite nucleation was considered in more detail, showing that inclusion particles can affect phase transformations by providing suitable nucleation sites. Different mechanisms were proposed. Abson, Dolby and Hart (Ref. 2) and Abson (Ref. 15) showed that the weld metal oxygen content affects mainly the position of the nucleation curve for the acicular ferrite phase field. Schematic CCT diagrams in Fig. 1 show the influence of weld metal oxygen on the austenite to ferrite phase transformation. The authors defined three regimes of transformation behavior with respect to the level of oxygen. In the low weld metal oxygen content regime (<200 ppm), acicular ferrite nucleation is restricted because of insufficient nucleants. As a result, Widmanstatten ferrite and bainite are the predominant microstructures — Fig. 1A. Ferrite nucleation probably occurred on inclusions associated with the austenite grain boundaries. In the intermediate weld metal oxygen content regime, intragranular acicular ferrite is the predominant microstructure. However, grain boundary ferrite, ferrite sideplates and sometimes bainite are also present — Fig. 1B. Nucleation probably occurred on inclusions lying at the prior austenite grain boundaries, resulting in grain boundary ferrites. Acicular ferrite was suggested to have nucleated on intragranular inclusions in a subsequent stage. In the high weld metal oxygen regime, inclusions lying within the grain boundaries are considered to be ferrite nucleation sites. It was suggested that the grain boundary ferrite nucleated and thickened in a direction perpendicular to the grain boundary. Widmanstatten sideplates, in the form of parallel laths, grow across the grain boundary. Some coarse intragranular laths may also be observed — Fig. 1C.

Cochrane and Kirkwood (Ref. 3) also suggested that oxygen in solution should not be considered as the primary variant, and that the early nucleation of primary ferrite at the austenite grain boundaries prior to the growth of the sideplates is in some way associated with the distribution and nature of weld metal inclusions in the higher oxygen deposits. Like Abson, *et al.* (Refs. 2, 15), they also raised the possibility of inclusion size distribution affecting the weld metal phase transformation.

Ricks, Barritte and Howell (Ref. 16) studied the influence of second phase particles on phase transformations in steels. They concluded that inert, nondeformable inclusions are always less effective sites for nucleation than grain boundaries. Nucleation on inclusions could only occur when site saturation of the boundaries had taken place.

Inclusion-assisted nucleation is a heterogeneous process in which interfacial energy at the nucleating interface is one of the major controlling factors. Lattice disregistry can be considered as one of the contributing factors. Disregistry can be expressed by the Turnbull equation:

$$\delta = \frac{\Delta a_o}{a_o} \qquad (1)$$

where Δa_o is the difference between the lattice parameters of the substrate and the nucleated solid for a low index plane, and a_o is the lattice parameter for the nucleated phase. Bramfitt (Ref. 17) modified Equation 1 and showed that the effectiveness of a compound as a nucleating agent is related to the lattice disregistry between the nucleating agent and the nucleating phase. The greater the disregistry between the substrate and the nucleating phase, the less effective the compound is in promoting nucleation.

Ito and Nakanishi (Ref. 18), Koukabi, *et al.* (Ref. 19), and Kanazawa, *et al.* (Ref. 20), suggested that TiN was an effective nucleating agent for acicular ferrite during the austenite decomposition. Heintze and McPherson (Ref. 21) reported the same findings, that TiN acted as a weld metal grain refining agent and that the effectiveness of titanium addition is enhanced in the presence of aluminum and boron.

However, Mori, *et al.* (Ref. 22), showed that an increase in nitrogen in the weld metal did not bring any microstructural change except for an increase in proeutectoid ferrite. Instead, they demonstrated that titanium containing oxides can nucleate acicular ferrite within the austenite grains. Using the model developed by Bramfitt (Ref. 17), the disregistries between several oxides and nitrides (the nucleating agents) and ferrite (the nucleated phase) were determined. Among the inclusions that were identified to be associated with high volume fractions of acicular ferrite, *i.e.,* Fe_3C, TiO, Ti_2O_3, $FeO \cdot TiO_2$, α-Al_2O_3, titanium monoxide has the smallest disregistry with ferrite, approximating three percent. They proposed then that titanium monoxide existed on the surface of oxide particles with high potency of nucleating acicular ferrite. However, no substantial experimental evidence could be supplied with respect to the surface titanium monoxide layer. Opposite to titanium monoxide, aluminum oxide and zirconium dioxide have the largest disregistries with nucleated ferrite, approximately 30 percent.

Along with the lattice disregistry model, the inclusions type was also considered to affect the weld metal ferrite formation. Keville and Cochrane (Ref. 23) determined that inclusions rich in aluminum oxide are typically related to welds which were made with basic fluxes, while aluminum oxide inclusions with MnS are associated with acidic fluxes. They suggested that the behavior can be related to weld pool deoxidation (Ref. 23). Using particle scanning electron microscopy, Pargeter (Ref. 24) determined the chemical compositions of the inclusions and observed the following relationships. Grain boundary ferrite and ferrite sideplates are usually associated with inclusions with manganese and silicon, with or without sulfur. Acicular ferrite appeared to be associated with aluminum-bearing particles.

Devillers, *et al.* (Ref. 25), found that acicular ferrite nucleated, in particular, at aluminum manganese silicate inclusions which were not covered by sulfur coating and which contained some titanium. Aluminum oxide particles were found, however, not to favor intragranular ferrite nucleation. Ricks, *et al.* (Ref. 26), detected the presence of manganese sulfide on the surface of some of the inclusions. They also observed a decrease in the inclusion titanium content in the sulfide coated particles. Cochrane, Ward and Keville (Ref. 27) and Sagesse, *et al.* (Ref. 28), reported that large proportions of acicular ferrite were obtained in the welds which contained stoichiometric alumina or alumina rich inclusions. These observations, sometimes contradictory, seem to indicate that the idea of specific types of inclusions being associated with particular microstructures may not be generally valid. Instead, it suggests that the effectiveness of inclusions on phase transformation behavior may depend on tramp elements (either in the form of surface coating or other ways) rather than on the macroanalysis of the inclusions.

It also became quite clear that acicular ferrite formation is a complex phenomenon with multiple factors and mechanisms operating simultaneously. Several other mechanisms suggested are summarized below. Harrison and Farrar (Ref. 29) correlated weld metal oxygen content with austenite grain size. A reduction in oxide inclusion content (by laser remelting of the weld metal) developed large austenite grain size, suggesting that the inclusions may have significant effect on the grain boundary pinning. They concluded that the austenite to ferrite transformation temperature change was due to the interaction of inclusions with austenite grain boundaries. Higher oxygen welds, *i.e.,* higher inclusion content, tend to reduce the austenite grain size and, therefore, favor high temperature transformation. Nucleation of acicular ferrite is aided by inclusions not associated with the prior austenite grain boundaries. Complete removal of the inclusions would lead to the development of bainite. Ferrante and Farrar (Ref. 30) also observed similar effects. They concluded that grains of diameters larger than 45 microns tended to produce acicular ferrite. Cochrane, Ward and Keville (Ref. 27), however, reported that for welds made on plates with a low aluminum level in spite of smaller austenite grain boundary surface areas, the austenite to ferrite transformation temperatures were observed to be lower. From this, they concluded that the grain boundary pinning is not the sole effect, and that the inclusion types present in the low aluminum weld are most effective in promoting ferrite nucleation at prior austenite grain boundaries.

Ferrante and Farrar (Ref. 30) reported that the mean inclusion diameter increased as the weld metal oxygen content increased. Cochrane, Ward and Keville (Ref. 27) also reported similar results. Ahlblom, *et al.* (Ref. 31), concluded in their recent publication that high fractions of acicular ferrite were often seen associated with small (average) diameter inclusions. They also found that the presence of rather coarse inclusions was generally associated with polygonal ferrite nucleation.

Another aspect that is often mentioned is that inclusions can accelerate nucleation through the difference in the thermal expansion behavior of the inclusions and matrix. The thermal expansion coefficient of the iron matrix (austenite) is much higher than that of the oxide inclusions (Ref. 32). During cooling, the austenite matrix is strained at the presence of inclusions and accelerates its transformation into ferrite. The local stresses around the inclusions can be so high that the matrix adjacent to the particles becomes plastically deformed. The lattice distortion in the vicinity of the dislocations can assist nucleation in various ways, namely, by reducing the total strain energy of the embryo and by providing growth enhancement of the embryo through the dislocation pipe diffusion mechanism. Considering the nature and magnitude of these stresses, Brooksbank and Andrews (Ref. 32) determined that such stress could also be responsible for crack initiation.

The main objective of this investigation is to examine in detail the effects of inclusions on HSLA steel weld metal phase transformation and to determine the influence of the inclusion size distribution on the austenite to ferrite transformation.

Experimental Procedure

The base metal chosen was a niobium microalloyed steel. Five commercial electrode wires were used to make the welds. The compositions of the base metal and the filler wires are given in Table 1. The CaF_2-CaO-SiO_2 flux system was selected because of its low oxygen activity and its ability to produce low oxygen welds. Based on the preliminary flux behavior studies (Ref. 33) and weld metal microstructural and toughness analyses results (Ref. 6) from bead-on-plate and double V-grooved welds, four fluxes were selected to perform a complete series of welding experiments producing different levels of weld metal oxygen contents—Fig. 2. For investigating the inclusions behavior only one set of data (welds made with Flux No. 13) will be discussed.

Single V-grooved welds were made on ½ in. (13 mm) thick 15 × 4.5 in. (380 × 110 mm) strips. In order to avoid contamination of the weld joints from mill scales, rust and edge preparation, the surfaces of the plates were also machined. The joint geometry is shown in Fig. 3. In addition to the welds mentioned above, a bead-on-plate weld made with commercial consumables (containing titanium, boron and other microalloying elements) using a heat input of 2.9 kJ/mm (74 kJ/in.) was also included in this study. The chemical composition of this second base metal and the titanium-boron electrode wire can also be found in Table 1. Together with other specifications, the welding variables used are listed in Table 2.

Quantitative metallography work was done on all the weldments. Transverse

Table 1—Chemical Compositions of the Base Metals and the Welding Consumables Used[a]

	C	Mn	Si	P	S	Cu	Cr	Ni	Mo	Al	Ti	Zr	B	V	Nb
Base Metal 1	0.140	1.250	0.220	0.008	0.008	0.210	0.140	0.170	0.030	0.019	–	–	–	–	0.029
E70S3	0.124	1.152	0.560	0.021	–	0.070	–	–	–	0.010	–	–	–	–	–
E70SG	0.066	1.690	0.610	0.016	0.028	0.020	–	–	–	0.010	–	–	–	–	–
EH 14	0.113	2.004	0.012	0.004	0.078	0.180	–	–	–	–	–	–	–	–	–
EM 5K	0.036	1.169	0.446	0.008	0.016	0.020	–	–	–	0.100	0.083	0.065	–	–	–
TiBOR 22	0.058	1.480	0.035	0.008	0.006	0.770	0.117	0.100	0.330	0.028	0.031	–	70	–	–
Base Metal 2	0.093	1.580	0.200	0.012	0.008	0.120	0.120	0.120	0.210	0.056	–	–	–	–	–

	SiO_2	Al_2O_3	MgO	CaO	MnO	TiO_2	CaF_2	Na_2O	Fe_2O_3	C
OP121 TT[b]	10.7	17.3	31.0	6.6	1.1	0.86	24.1	0.78	1.9	0.35

[a]Concentration expressed in weight percent, except boron—ppm.
[b]Typical analysis.

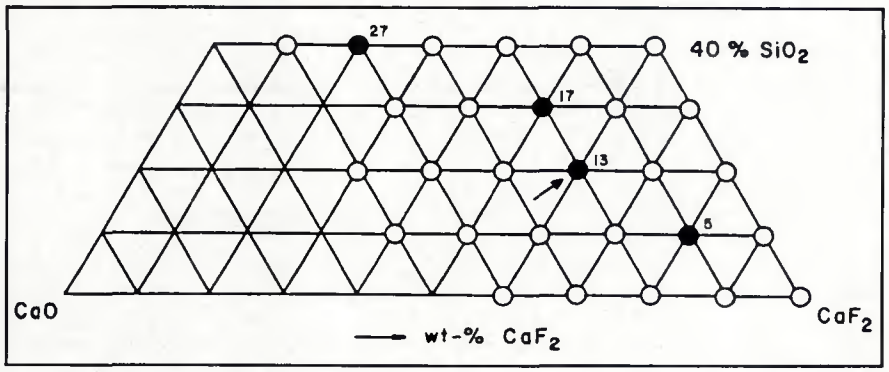

Fig. 2—Partial ternary diagram for CaF_2-CaO-SiO_2 system showing the nominal compositions of the 28 fluxes melted. (●—Fluxes used in welding experiments)

sections were cut and their surfaces prepared for metallographic examination. The metallographic study also involved prior austenite grain size determination. Due to sectioning orientation effect, the measurement on a transverse section may not correspond to the true austenite grain size. Therefore, sections parallel to the fusion line (perpendicular to the columnar grains) were prepared and approximately equiaxed austenite grains were observed and measured. Figure 4 shows this section view with the delineated equiaxed grain structure. Thermal grooving techniques were also used to duplicate the grain size measurements.

High magnification light micrographs of polished and unetched weld samples were obtained for the inclusion analyses. The values determined by light microscopy for the inclusions volume fraction, areal density, and linear density were too low and consequently not used for further analysis.

Carbon extraction replicas were made on the welds in order to examine the inclusions and other second phases. A Phillips 400 TEM was used in the determination of the sizes, number densities, volume fractions, and the geometrical shapes of the inclusions. The phases associated with the inclusions were also examined. For the size distribution determination and the calculation of volume fraction, number density, and the mean particle size of the inclusions, the Ashby and Ebeling equations (Ref. 34) were used.

Chemical analyses of the welds were performed with a Baird Atomic Spectrovac Model 1000 emission spectrometer. Weld metal oxygen, nitrogen and carbon contents were determined using Leco interstitial analyzers.

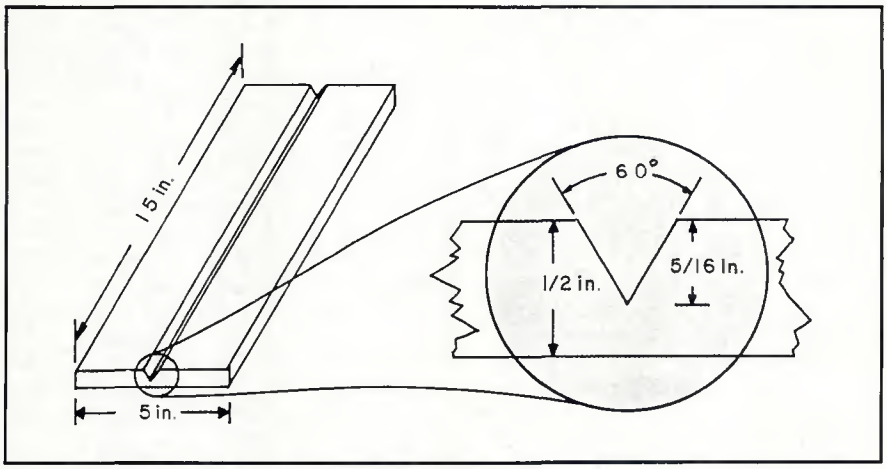

Fig. 3—Joint geometry of the single V-groove welds

Results and Discussion

To study the relationship between weld metal composition and microstructure, carbon equivalent type equations were used. Several different forms of CE equations (Refs. 35–39) can be found in the literature, but only the P_{cm} equation

$$P_{cm} = C + \frac{Mn + Cr + Cu}{20} + \frac{Si}{30} + \frac{V}{10} + \frac{Mo}{15} + \frac{Ni}{60} + 5B \quad (2)$$

where the elements are represented in weight percent, was included in this discussion because it covers the major elements in the weld metal. Most of the CE type equations do not take into consideration the weld cooling rate, prior austenite grain size, inclusion effects, etc., but literature data (Refs. 27, 40) showed a clear trend that with increasing carbon equivalent, there is an initial increase in the acicular ferrite content, followed by progressively increasing amounts of bainite and martensite.

Table 2—Operating Variables Used to Make the Weld Specimens for this Inclusion Investigation

	E70S3	E70SG	EH 14	EM 5K	TiBOR 22
Base Metal 1 Flux 13	S313H	SG13H	EH13H	EM13H	Ti13H
	Welding Current: 310 A Welding Voltage: 35 V		Travel Speed: 4.4 mm/s Heat Input: 2.5 kJ/mm (62 kJ/in.)		
Base Metal 2 OP121 TT			TiBOR 22 TiOeH		
	Welding Current: 530 A Welding Voltage: 30 V		Travel Speed: 5.2 mm/s Heat Input: 3.0 kJ/mm (76 kJ/in.)		

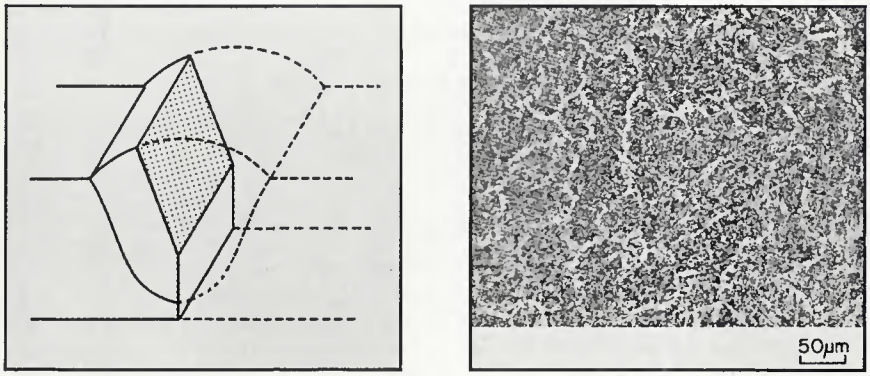

Fig. 4—Schematic diagram and light micrograph showing the sample preparation and the microstructural aspects of prior austenite grain size determination

The same tendency, however, was not observed in this work. Figure 5 is a plot showing the correlation between volume fraction of acicular ferrite and P_{cm}. Within the range of P_{cm} values considered, a large scatter in acicular ferrite was observed, from 40 to above 80 percent. In other words, P_{cm} alone is insufficient to characterize the weld metal microstructure, even when the cooling rate is maintained constant, as in the weldments under investigation. Two representative weld metal micrographs of low and high volume fraction of acicular ferrite are shown in Fig. 6.

For a similar chemical composition and cooling rate, larger austenite grain size steels usually show higher hardenability due to a smaller grain surface area to volume ratio (lower surface nucleation site availability). Consequently, less grain boundary ferrite can be expected in the final microstructure. Volume fractions of primary ferrite (here defined as the sum of grain boundary ferrite and Widmanstatten sideplates) were plotted in Fig. 7 as a function of measured prior austenite grain sizes. With increasing prior austenite grain size, the amount of primary ferrite was observed to decrease. In the case of acicular ferrite, the opposite trend appeared to be true, although with a larger scatter. However, examining the welds SG13H, Ti13H and TiOeH, which showed similar P_{cm} and prior austenite grain sizes, the weld metal microstructures were very different, varying from 40 to above 80 percent of acicular ferrite. This indicates that some other factors (or combination of factors) must also contribute to the final microstructure.

The grain boundary ferrite transformation can be described as a two step process:

1) Nucleation along the austenite grain boundaries.
2) Growth in a direction perpendicular to the interface, into the austenite grain.

If nucleation is assumed to be easy and site saturation occurs readily, the problem in question resembles that of surface nucleation where the grain surface will be covered by a layer of transformed material. Further assumptions made are that allotriomorph growth is diffusion controlled and that austenite grains are cylindrical in shape. Using the Avrami type equation approach, the following expression was obtained:

$$X = 1 - \exp\left(\frac{-3\sqrt{t}}{d}\right) \qquad (3)$$

where X is the volume fraction of grain boundary ferrite transformed, t is the cooling time from 800° to 500°C (1472°

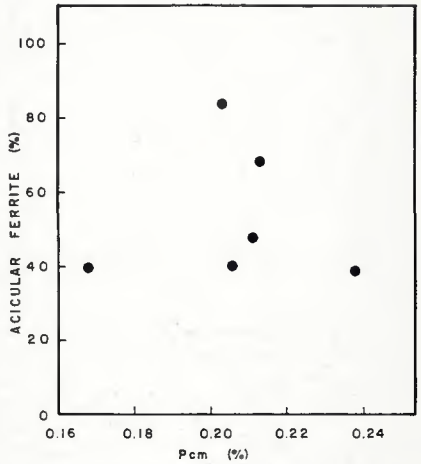

Fig. 5—Effect of P_{cm} on the weld metal acicular ferrite content

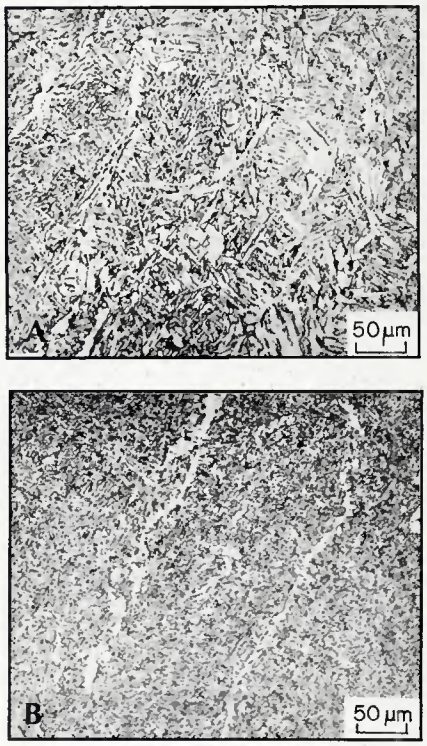

Fig. 6—Light micrographs illustrating the low and high volume fractions of acicular ferrite microstructures. A—S313H weld; B—TiOeH weld

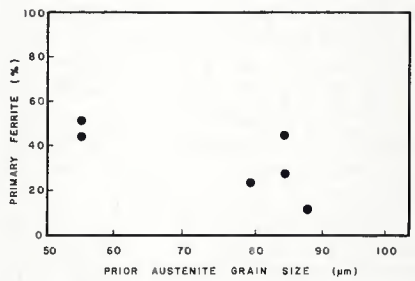

Fig. 7—Effects of prior austenite grain size on the weld metal primary ferrite content

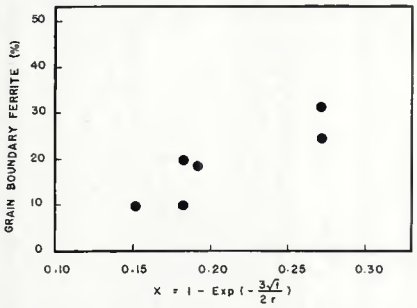

Fig. 8 — Correlation between experimentally measured and calculated amounts of transformed grain boundary ferrite

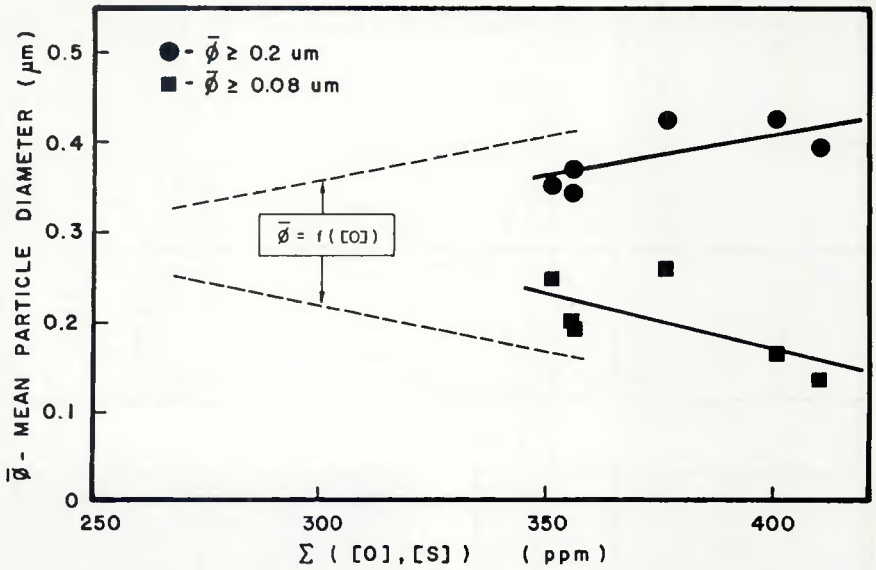

Fig. 9 — Variation of mean particle size of the inclusions with weld metal oxygen and sulfur content

to 932°F), and d is the prior austenite grain diameter. As mentioned previously, every effort has been made to minimize the sectioning orientation effect in the austenite grain size determination such that imprecision involved in the quantitative metallography procedure will only affect slightly the coefficient and the calculation of the equation.

Experimentally measured volume fractions of grain boundary ferrite were plotted against the calculated values of X in Fig. 8. Good correlation was obtained, indicating that the grain boundary ferrite formation can be described by Equation 3. Nucleation originated on the austenite grain boundaries, and the more the grain boundary ferrite grows into the austenite grain, the smaller will be the intragranular region left for acicular ferrite. In the case of high acicular ferrite content welds, this also seems to suggest a much earlier involvement of the intragranular inclusions in the weld metal phase transformation in blocking any further growth of the allotriomorphs.

For a better understanding of the weld metal phase transformation, one needs to analyze more closely all the factors that will affect the austenite to ferrite transformation. In addition to the weld metal chemical hardenability, the cooling rate, and the prior austenite grain size, the presence of weld metal inclusions and their effects on the austenite decomposition should also be emphasized. Inclusions may affect both the thermodynamic and kinetic aspects of the weld metal transformations. First, the inclusions provide nucleation sites for the ferrite formation and alter the kinetic condition of the process. Second, due to the differential thermal contraction between the matrix and the inclusions, the austenite matrix becomes strained during cooling, thus increasing the thermodynamic desire for the austenite to transform into ferrite.

Inclusion parameters such as mean particle size and particle size mode (the highest frequency class in the distribution), volume fraction, number density, and size distribution are all fundamentally important in weld metal phase transformation.

As was reported in the introduction (Refs. 27, 30, 31), the mean inclusion diameter was observed to increase with an increasing weld metal oxygen. An analysis of the transmission electron micrographs of the replicas in this work showed that such observation could not be verified. Higher weld metal oxygen samples indeed resulted in higher inclusion content than the lower oxygen welds. However, finer particles and larger size variation were also seen in the higher oxygen EM13H and S313H weld specimens. This seems to agree with previous observations reported by Dallam, *et al.* (Ref. 6).

To verify the relationship between mean particle diameter and the main inclusion-forming elements in the weld metal (oxygen and sulfur), a linear regression analysis was performed and the results are shown in Fig. 9. The straight line passing through the full square points represents all the inclusions measured in this work, *i.e.*, particles with diameters > 0.07 micron. It showed that the mean particle size decreased with an increasing concentration of oxygen and sulfur. This observation is different from what was reported in the literature (Refs. 25, 28). Suspecting that the disagreement might be due to the sampling and the smallest size particles included in the studies, inclusions smaller than 0.2 micron were excluded in a second calculation. This set of calculated values was plotted in the same chart as full circles. This slope of the regression line is now positive, indicating that particle size increased with increasing concentration of oxygen and sulfur. Nucleation rate is exponentially proportional to the inverse of the free energy change of the inclusion formation, which is a function of the weld metal oxygen and sulfur content. Therefore, the higher the concentration of the inclusion formers, the larger will be the number of nuclei formed. Given the same period of time of coalescence in the melt, the weld metal with the larger number of nuclei will average smaller size particles. The effects of number of nuclei in the melt on the rate of growth of oxide inclusions were discussed thoroughly in the literature (Refs. 41–44) and seem to agree with the present observation.

Inclusion volume fraction and number density were plotted as functions of weld metal oxygen and sulfur content. Figure 10 shows the results of such correlation. Inclusion volume fraction and number density both increased with increasing weld metal oxygen and sulfur content.

The influence of inclusions on weld metal transformations can be explained in two ways. First, they are concentrated in the grain boundary region, pinning the austenite grain boundary and providing nucleation sites. Too high inclusion density would lead to a more restricted austenite grain growth, resulting in a very large surface area to volume ratio. This increases the possibility of grain boundary ferrite occurrence. On the other hand, a large austenite grain increases the hardenability of the weld metal by affecting the kinetic feasibility of grain boundary ferrite formation. To verify whether inclusions were pinning the prior austenite grain boundaries or not, the relationship between the prior austenite grain size and inclusion number density was represented graphically in Fig. 11. Very good correlation was obtained, indicating that weld metal oxygen and sulfur expressed as number of inclusions did

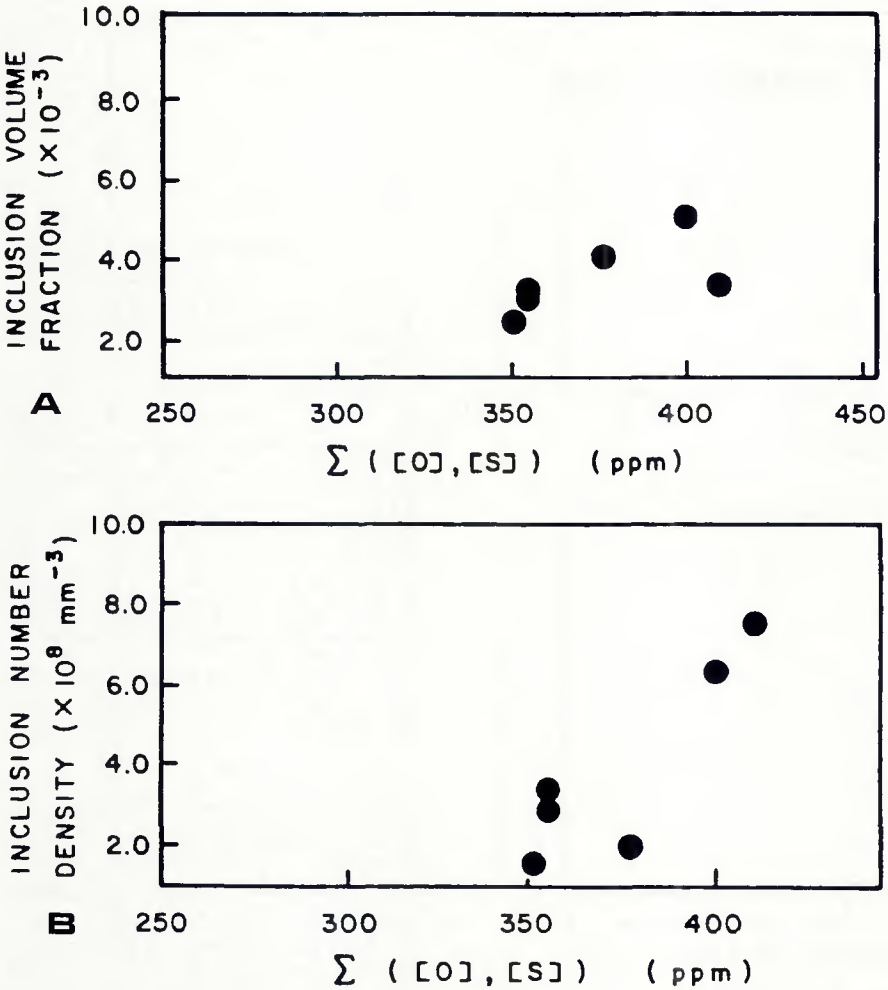

Fig. 10 — Effects of weld metal oxygen and sulfur content on the inclusions volume fraction and number density

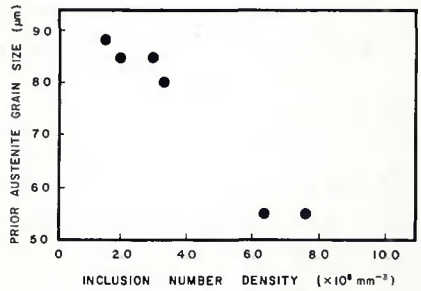

Fig. 11 — Effects of inclusion number density on the prior austenite grain size in the weld metal

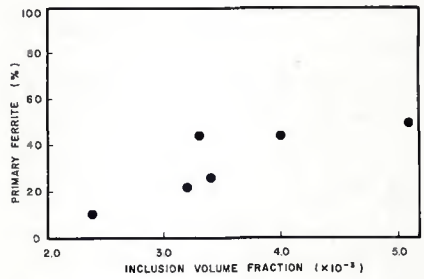

Fig. 12 — Variation of the percent of weld metal primary ferrite with the inclusion volume fraction

affect the prior austenite grain size. Second, the inclusions that are within the austenite grains will provide nucleation sites for acicular ferrite formation, and an adequate inclusion density is needed to obtain short, randomly oriented acicular laths. A low inclusion density would lead to a larger extent of ferrite lath growth, resulting in longer needles before they impinge on each other. Figure 12 illustrates the variation of the percentage of primary ferrite with the inclusion volume fraction. A general trend of primary ferrite increase was observed with the increasing inclusion density.

Combining the results from Figs. 10–12, one can realize that the relationship between weld metal oxygen and weld metal microstructure is only an indirect one. It could be used to describe the weld metal microstructure transition with reasonable success solely because the weld metal inclusion population is directly proportional to the weld metal oxygen content, since it is the main inclusion former.

For a more complete understanding of the role of inclusions in weld metal phase transformation, the inclusion size distribution and their effects have also to be considered. The inclusion size distributions of the different welds were determined. Basically, two types of distributions were observed. They are the reverse J-shaped distribution and the positively skewed, or right skewed, distribution. The first type was represented by the welds S313H and EM13H — Fig. 13A. The second type included the SG13H, EH13H, Ti13H and TiOeH welds — Fig. 13B. Among the welds from the second group, inclusion populations in Ti13H and TiOeH approximated more closely the normal distribution, showing larger particle size modes (0.25 and 0.35 micron, respectively) and also larger mean particle sizes (0.21 and 0.24 micron, respectively). Different from some previous observations (Ref. 27), *i.e.*, in spite of the larger inclusions sizes, these weld specimens showed the finest microstructures, predominantly acicular ferrite. Figure 14 shows the effect of inclusion particle size on acicular ferrite content.

The inclusion size distribution effect can also be seen in the first group of weld metals. Both S313H and EM13H welds showed very high occurrence frequency of small size particles. Approximately 50 and 30 percent, respectively, of particles < 0.1 micron could be found. The mean particle sizes of the inclusions were also extremely fine, 0.14 and 0.16 micron, respectively. Those were also the welds that presented larger volumes of grain boundary ferrite. This is reasonable because smaller particles more effectively pin the prior austenite grain boundaries, resulting in smaller austenite grain sizes, as shown in Fig. 15. Consequently, more grain boundary allotriomorph would be expected. This also shows that the pinning of austenite grain boundary by inclusions not only depends on the volume fraction, but also varies with size distribution. Zener's equation (Ref. 45)

$$D_L = \text{Limiting Grain Size} = \frac{2d_{cr}}{3f} \qquad (4)$$

describes the effectiveness of inclusions pinning grain boundaries. Given the austenite grain size and the inclusion volume fraction, f, the critical inclusion size, d_{cr} (above which inclusions will not restrain grain growth), can be calculated. The determined values of d_{cr} can be found in Table 3. To relate this to the measured size distributions, the critical inclusion sizes were used to determine the fraction of inclusions associated with the grain boundaries (F). Multiplying the total num-

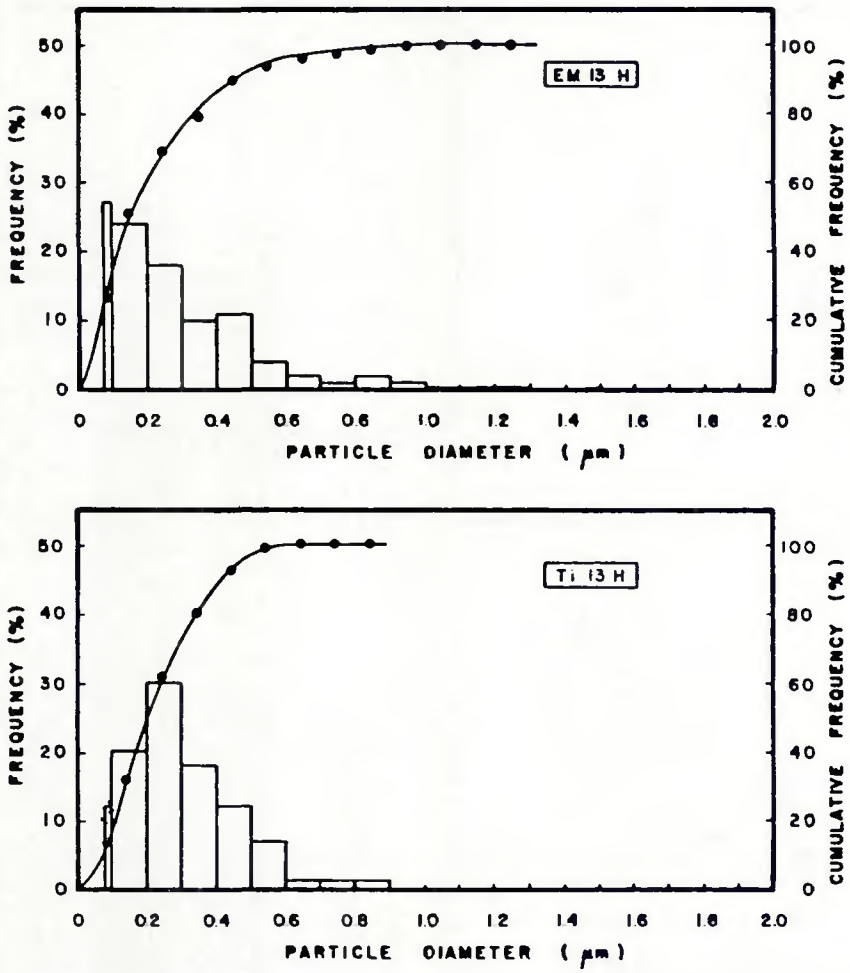

Fig. 13 — Simple and cumulative size distribution of the inclusions extracted from EM13H and Ti13H weld metal

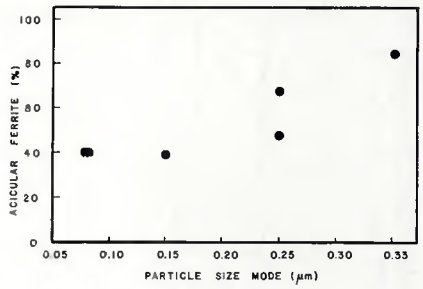

Fig. 14 — Effects of inclusion particle size mode on the percent of acicular ferrite in the weld metal

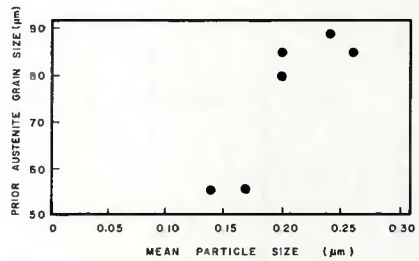

Fig. 15 — Variation of prior austenite grain size with the mean particle size of the inclusions

ber density (N_v) by the fraction (F), the inclusion density associated with the prior austenite grain boundaries (n_b) is determined. Prior austenite grain size is plotted as a function of the inclusions found in the boundaries in Fig. 16. The excellent correlation indicates that the inclusion size distribution effect determines the number of inclusions in the boundaries, indirectly controlling the austenite grain size. The difference between N_v and n_b is the intragranular inclusion density, n_i, *i.e.*, the potential sites for ferrite nucleation within the grains. The larger number of intragranular inclusions in S313H and EM13H weld metals did not guarantee a high acicular ferrite content. This is because of the smaller prior austenite grain size (held by the extremely large number of small inclusions associated with the grain boundaries), providing conditions for the grain boundary allotriomorphs to nucleate and grow. Once the grain boundary ferrite is formed, it decreases the physical space in the grain interior for acicular ferrite to form and grow. In the case of EH13H weld, the number of intragranular inclusions seems to be low, with a calculated mean free spacing between inclusions of approximately five microns, allowing the ferrite laths to grow. However, the formation of bainite is also due to the higher chemical hardenability found in the weldment. In the other direction are the specimens Ti13H and TiOeH, which showed slightly higher intragranular inclusion density than the EH13H weld. The calculated mean free spacing between laths is only two microns. Because of that, more ferrite laths may nucleate and grow to impingement, resulting in a much finer microstructure with higher acicular ferrite content. The inclusion size distribution effect can also be seen in Fig. 17, where acicular ferrite content is plotted as a function of intragranular inclusion density. The maximum acicular ferrite content corresponds to the welds with the optimum inclusion size distributions.

Table 3—Summary of the Results of Calculation of the Critical Inclusion Sizes (d_{cr}) and the Inclusion Densities Associated with Austenite Grain Boundaries and Interior of Grains

	γ_{gs} (μm)	f	d_{cr} (μm)	N_v (10^8 mm^{-3})	F	n_b (10^8 mm^{-3})	$N_v - n_b$ (10^8 mm^{-3})
S313H	55	0.033	0.27	7.60	0.82	6.23	1.37
SG13H	85	0.0040	0.51	2.01	0.85	1.71	0.30
EH13H	85	0.033	0.42	2.99	0.88	2.63	0.36
EM13H	55	0.0051	0.42	6.40	0.87	5.57	0.83
Ti13H	80	0.0033	0.40	3.27	0.86	2.81	0.46
TiOeH	88	0.0025	0.33	1.54	0.72	1.11	0.43

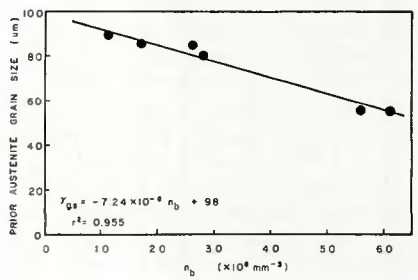

Fig. 16 — Effects of inclusions associated with the grain boundaries on the prior austenite grain size

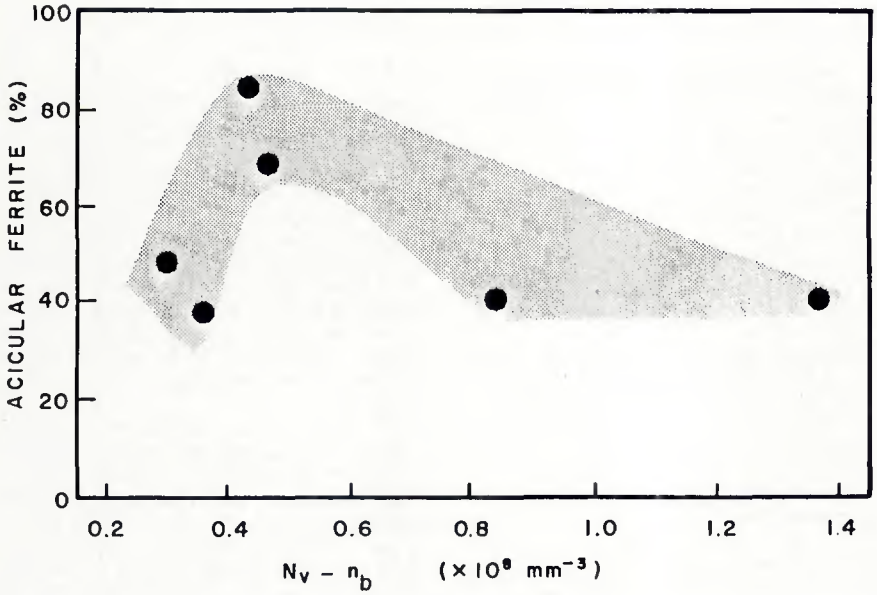

Fig. 17 — Variation of weld metal acicular ferrite content with the number density of intragranular inclusions

Fig. 18 — TEM micrograph of weld metal carbon extraction replica showing inclusions as nucleation sites for acicular ferrite laths

In order to obtain a fine microstructure with high acicular ferrite content, the weld metal has to have an adequate prior austenite grain size and optimum intragranular inclusion density. Too few inclusions will provide large austenite grains but fewer intragranular nucleation sites with chances for the ferrite to grow more before impingement, resulting in bainite type of microstructures. A large population of smaller inclusions will pin the boundaries so much that fine austenite grain size will develop. This provides excellent conditions for the growth of allotriomorphs, even before the acicular ferrite could have a chance to nucleate or grow. Therefore, weld metals characterized by size distributions with a large number of fine particles usually show fine austenite grain size and coarse microstructure composed of grain boundary ferrite and some acicular ferrite.

To evaluate the effects of inclusion/matrix differential thermal contraction on weld metal phase transformation, "a ball in elastic hole" model was considered (Ref. 46). At temperatures slightly below the solidification point, it is reasonable to assume that the sizes of the inclusion (ball) and hole in the matrix are the same. During cooling, because of the different thermal expansion coefficients, the inclusion and the matrix will contract to different degrees. Generally, thermal expansion coefficients of nonmetallic inclusions are smaller than that of the austenite matrix. Therefore, at any temperature in the later stages of cooling, the hole will be smaller than the inclusion. Assuming that continuity will be maintained across the inclusion/matrix interface, the differential thermal contraction described above will generate strain and stress fields in the austenite.

If the inclusion is assumed to be a rigid sphere, incompressible and nondeformable, the austenite will take all the strain during cooling. The total strain energy in the matrix is estimated by calculating the work done on the hole surface. When the calculated strain energy values associated with the presence of inclusions (approximately 0.5 J/cm^3) are compared with the austenite to ferrite transformation free energy change (approximately 100 J/cm^3 in low carbon steels), they showed several orders of magnitude difference, indicating that the strain energy term is probably insignificant in the overall reaction. Another explanation would be that the "ball in elastic hole" model is too simplistic and does not take into consideration the anisotropic nature of the elastic constants. The crystal structure change would generate other forms of distortion energy which would be more significant and would add to the strain energy term in the free energy equation.

Summarizing the discussion, austenite decomposition can be described as follows. Oxygen affects the weld metal phase transformation in the form of inclusions, such as oxides and oxy-sulfides. These inclusions can locate both at austenite grain boundaries and intragranularly. Depending on their location, they may have different functions. Small inclusions more effectively pin the boundaries in the cooling cycle, therefore particles with diameters smaller than the critical size will be more often found at the boundaries. Since ferrite nucleation at grain boundaries is very favorable, site saturation soon occurs. This is followed by extensive allotriomorphic growth. Spaces that are not occupied by grain boundary ferrite are later available for acicular ferrite and other transformation products. Intragranular inclusions provide the initial nucleation sites for acicular ferrite formation, as shown in Fig. 18. This evidence is supported by other authors (Refs. 30, 47–49). Sympathetic nucleation may occur at later stages (Refs. 16, 24–26, 47, 48). Size distribution is important to determine the number of inclusions located intragranularly. An optimum size distribution will result in an optimum inclusion number density within the austenite grains.

This inclusion size distribution effect can also explain the enhancement in microstructural refinement brought about by boron. Boron migrates to the grain boundaries, poisoning the available sites for allotriomorphic ferrite nucleation. This decreases the grain boundary ferrite content. At the same time, chances increase for the intragranular inclusion to nucleate ferrite. With adequate prior austenite grain size and chemical hardenability, the acicular ferrite content can be maximized.

Conclusions

The major achievements of this investigation can be summarized in the following conclusions:

1. Inclusion volume fraction can be directly related to the concentration of inclusion formers (mainly oxygen and sulfur) and does affect the austenite to

ferrite transformation.

2. Grain boundary allotriomorph growth is diffusion controlled and can be described by an Avrami type equation as a function of prior austenite grain size and cooling rate.

3. The inclusion size distribution determines whether the inclusions will be associated with grain boundaries or located intragranularly, controlling the final weld metal microstructure.

4. Weld metals with high acicular ferrite content are found to be associated with coarse austenite grains and with a large number of inclusions of diameters > 0.2 micron.

5. High oxygen content weld metals with higher grain boundary ferrite content are found to be associated with fine austenite grains and with a large number of smaller size inclusions of diameters < 0.1 micron.

6. As weld metal oxygen content increases, the mean particle size of the inclusions decreases because of a higher occurrence frequency of very fine particles of diameters < 0.1 micron.

Acknowledgments

The authors acknowledge the research and fellowship support of the United States Army Research Office, the Conselho Nacional de Pesquisa e Desenvolvimento do Brasil, and the material and equipment support of Lukens Steel Company and Hobart Brothers Company.

References

1. Glover, A.G., McGrath, J.T., Tinkler, M.J., and Weatherly, G.C. 1977. The influence of cooling rate and composition on weld metal microstructure in C-Mn HSLA steel. *Welding Journal* 56(9):267-s to 273-s.

2. Abson, D.J., Dolby, R.E., and Hart, P.H.M. 1978. The role of non-metallic inclusions in ferrite nucleation in carbon steel weld metals. Proc. Intl. Conf. on *Trends in Steels and Consumables for Welding,* London, England, The Welding Institute, p. 75.

3. Cochrane, R.C., and Kirkwood, P.R. 1978. The effect of oxygen on weld metal microstructure. Proc. Intl. Conf. on *Trends in Steels and Consumables for Welding,* London, England, The Welding Institute, p. 103.

4. North, T.H., Bell, H.B., Koukabi, A., and Craig, I. 1979. Notch toughness of low oxygen content submerged arc deposits. *Welding Journal* 58(12):343-s to 354-s.

5. Dolby, R.E. 1976. *Factors Controlling Weld Toughness – The Present Position. Part II – Weld Metals.* The Welding Institute, Cambridge, England.

6. Dallam, C.B., Liu, S., and Olson, D.L. 1985. Flux composition dependence of microstructure and toughness of submerged arc HSLA weldments. *Welding Journal* 64(5):140-s to 151-s.

7. Grong, O., Siewert, T.A., Martins, G.P., and Olson, D.L. 1985. A model for the sequence of reactions occurring during silicon-manganese deoxidation of mild and low alloy steel weld metals. Submitted for publication.

8. Lau, T.W., and HoSang, A. 1984. Inclusion study, research report. Welding Institute of Canada, RC200/2/84.

9. Irvine, K.J., and Pickering, F.B. 1960. Relationship between microstructure and mechanical properties of mild steel weld deposits. *British Welding Journal* 7:353.

10. Wheatley, J.M., and Baker, R.G. 1962. Mechanical properties of a mild steel weld metal deposited by the metal-arc process. *British Welding Journal* 9:378.

11. Gloor, K., Christensen, N., Maehle, G., and Simonsen, T. 1963. Non-metallic inclusions in weld metal. IIW DOC II-A-106-63.

12. Tichelaar, G.W. 1964. Brittle fracture of mild steel weld metal at low temperatures. Proc. Welding Symposium, Rotterdam, p. 31.

13. Katoh, K. 1965. Investigation of non-metallic inclusions in mild steel weld metals. IIW DOC II-A-158-65.

14. Boniszewski, T. 1972. Fine oxide particles in mild steel CO_2 weld metal. *Welding Journal* 51(1):19-s to 22-s.

15. Abson, D.J. 1978. *The Role of Inclusions in Controlling Weld Metal Microstructures in C-Mn Steels.* The Welding Institute, Cambridge, England

16. Ricks, R.A., Barritte, G.S., and Howell, P.R. 1981. The influence of second phase particles on diffusional phase transformations in steels. Proc. Intl. Conf. on *Solid State Phase Transformations,* Pittsburgh, Pa., AIME, p. 463.

17. Bramfitt, B.L. 1970. The effect of carbide and nitride additions on the heterogeneous nucleation behavior of liquid iron. *Metallurgical Transactions* 1A (1):1987.

18. Ito, Y., and Nakanishi, M. 1976. Study on Charpy impact properties of weld metals with submerged arc welding. *The Sumitomo Search* 15:42.

19. Koukabi, A., North, T.H., and Bell, H.B. 1978. Flux formation, sulphur, oxygen and rare-earth additions in submerged arc welding. Proc. Intl. Conf. on *Trends in Steels and Consumables for Welding,* London, England, The Welding Institute, p. 281.

20. Kanazawa, S., Nakashima, A., Okamoto, K., and Kanaya, K. 1976. Improvement of weld fusion zone toughness by fine TiN. *Transactions ISIJ* 16:486.

21. Heintze, G.W., and McPherson, R. 1983. Grain refinement of steels by titanium innoculation during submerged arc welding. *Australian Welding Journal* 28:37.

22. Mori, N., Homma, H., Okita, S., and Asano, K. 1980. The behavior of B and N in notch toughness improvement of Ti-B bearing weld metals. IIW DOC IX-1158-80.

23. Keville, B.R., and Cochrane, R.C. 1982. Factors controlling the microstructure and toughness of submerged arc weldments. Proc. 30th Annual Convention on *Welding Technology 82,* Hobart, The Australian Welding Institute, p. 263.

24. Pargeter, R.J. 1981. *Investigation of Submerged Arc Weld Metal Inclusions.* The Welding Institute, Cambridge, England.

25. Devillers, L., Kaplan, D., Marandet, B., Ribes, A., and Riboud, P.V. 1983. The effect of low level concentrations of some elements on the toughness of submerged arc welded C-Mn welds. Proc. Intl. Conf. on *The Effects of Residual, Impurity and Micro-alloying Elements on Weldability and Weld Properties,* London, England, The Welding Institute, p. 1.

26. Ricks, R.A., Howell, P.R., and Barritte, G.S. 1982. The nature of acicular ferrite in HSLA steel weld metals. *Journal of Materials Science* 17:732.

27. Cochrane, R.C., Ward, J.L., and Keville, B.R. 1983. The influence of deoxidation and/or desulphurisation practice on the weld metal toughness of high dilution welds. Proc. Intl. Conf. on *The Effects of Residual, Impurity and Micro-alloying Elements on Weldability and Weld Properties,* London, England, The Welding Institute, Paper 16.

28. Saggesse, M.E., Bhatti, A.R., Hawkins, D.N., and Whiteman, J.A. 1983. Factors influencing inclusions chemistry and microstructure in submerged arc welds. Proc. Intl. Conf. on *The Effects of Residual, Impurity and Micro-alloying Elements on Weldability and Weld Properties,* London, England, The Welding Institute, Paper 15.

29. Harrison, P.L., and Farrar, R.A. 1981. Influence of oxygen-rich inclusions on the austenite to ferrite phase transformation in high-strength low-alloy (HSLA) steel weld metals. *Journal of Materials Science* 16:2218.

30. Ferrante, M., and Farrar, R.A. 1982. The role of oxygen rich inclusions in determining the microstructure of weld metal deposits. *Journal of Materials Science* 17:3293.

31. Ahlblom, B., Bergstrom, H., Hannerz, N.E., and Werlefors, I. 1983. Influence of welding parameters on nitrogen content and microstructure of submerged arc weld metal. Proc. Intl. Conf. on *The Effects of Residual, Impurity and Micro-alloying Elements on Weldability and Weld Properties,* London, England, The Welding Institute, Paper 38.

32. Brooksbank, D., and Andrews, K.W. 1972. Stress fields around inclusions and their relation to mechanical properties. *Journal of the Iron and Steel Institute* 210:246.

33. Liu, S., Dallam, C.B., and Olson, D.L. 1982. Performance of the CaF_2-CaO-SiO_2 system as a submerged arc welding flux for a niobium based HSLA steel. Proc. of ASM Intl. Conf. on *Welding Technology for Energy Applications,* Gatlinburg, Tenn., p. 445.

34. Ashby, M.F., and Ebeling, R. 1966. On the deformation of the number, size, spacing, and volume fraction of spherical second phase particles from extraction replicas. *Trans. AIME.* 236:1396.

35. Granjon, H. 1967. Note on the carbon equivalent. IIW DOC IX-555-67.

36. Ito, Y., and Bessyo, K. 1968. Weldability formula of high strength steel related to heat affected zone cracking. IIW DOC IX-576-68.

37. Duren, C.F. 1977. Significance of the implant test for assessment of the field weldability of large diameter pipes. *Mannessmann Research Institute Report,* Duisberg, PRG.

38. Tanaka, J., and Kitada, T. 1976. Implant test for studying cold cracking. IIW DOC IX-959-76.

39. Sekiguchi, H. 1976. Fundamental research on the welding heat affected zone of steels. Nikkan Kogyo Shimbum, Tokyo, Japan.

40. Graville, B.A. 1980. Factors affecting the toughness of submerged arc weld metal – part II. *Technology Focus – Welding Institute of Canada* 2:1.

41. Kiessling, R. 1978. *Non-Metallic Inclusions in Steel Parts I-IV,* London, England, The Metal Society.

42. Twidwell, L.G. *Physical Chemistry of Iron and Steelmaking.* Butte, Mont., College of Mineral Science and Technology.

43. U.S. Steel Corporation. 1971. *The Making, Shaping, and Treating of Steels.* 9th Edi-

tion, Pittsburgh, Pa., p. 281.
44. Turkdogan, E.T. 1972. Deoxidation of steel. *Journal of The Iron and Steel Institute* 210:21.
45. Smith, C.S. 1948. Grains, phases and interfaces: an interpretation of microstructures. *Trans. AIME* 175:15.
46. Hirth, J.P., and Lothe, J. 1982. *Theory of Dislocations*, pp. 30–58, New York, N.Y., McGraw Hill.
47. Barritte, G.S., Ricks, R.A., and Howell, P.R. 1981. Application of STEM/EDS to study of microstructural development in HSLA steel weld metals. Proc. on *Quantitative Microanalysis with High Spatial Resolution*, London, England, The Metals Society, p. 122.
48. Kayali, E.S., Corbett, J.M., and Kerr, H.W. 1983. Observations on inclusions and acicular ferrite nucleation in submerged arc HSLA welds. *Journal of Materials Science Letters* 2:123.
49. Indacochea, J.E., and Olson, D.L. 1983. Relationship of weld metal microstructure and penetration to weld metal oxygen content. *Journal of Materials for Energy Systems* 5:139.

WRC Bulletin 309
November 1985

Development of a Production Test Procedure for Gaskets
By A. Bazergui, L. Marchand and H. D. Raut

This report presents detailed results of tests carried out on five styles of gaskets with properties covering the broad range of gaskets commercially available. Three types of tests have been performed: mechanical (stress-deflection and creep); leakage tests on a hydraulic test rig; and leakage tests on a bolted-up rig. The report also presents selected Milestone Gasket Test Program results which pertain to four other styles of gaskets.

The publication of this report was sponsored by the Task Group on Gasket Testing of the Subcommittee on Bolted Flanged Connections of the Welding Research Council. The price of WRC Bulletin 309 is $14.00 per copy, plus $5.00 for postage and handling. Orders should be sent with payment to the Welding Research Council, Ste. 1301, 345 E. 47th St., New York, NY 10017.

WRC Bulletin 310
December 1985

Damage Studies in Pressure Vessel Components
By F. A. Leckie

The theory of damage mechanics is applied to pressure vessel components operating at high temperatures. It is suggested that some existing design procedures can be readily adapted to deal with high temperature problems.

The publication of this report was sponsored by the Subcommittee on Elevated Temperature Design of the Pressure Vessel Research Committee of the Welding Research Council. The price of WRC Bulletin 310 is $14.00 per copy, plus $5.00 for postage and handling. Orders should be sent with payment to the Welding Research Council, Ste. 1301, 345 E. 47th St., New York, NY 10017.

WRC Bulletin 311
January 1986

Assessment of the Significance of Weld Discontinuities: Effects of Microstructure and Discontinuities upon Fracture Morphology
By C. D. Lundin and C. R. Patriarca

The purpose of this report was to systematically investigate the metallurgical influence of weld metal microstructure, hydrogen presence and loading rate on fracture morphology in the presence of different types of discontinuities. In order to assess the metallurgical significance of weld discontinuities on fracture characteristics, mechanical and nondestructive testing, metallographic and fractographic examination, and hydrogen determinations were used to evaluate E7018, E9018 and E11018 weld metals.

Publication of this report was sponsored by the Subcommittee on Significance of Weld Discontinuities of the Pressure Vessel Research Committee of the Welding Research Council. The price of WRC Bulletin 311 is $14.00 per copy, plus $5.00 for postage and handling. Orders should be sent with payment to the Welding Research Council, Ste. 1301, 345 E. 47th St., New York, NY 10017.